agronomy

MDPI

Article

Design of Vegetation Index for Identifying the Mosaic Virus in Sugarcane Plantation: A Brazilian Case Study

Érika Akemi Saito Moriya [1], Nilton Nobuhiro Imai [1], Antonio Maria Garcia Tommaselli [1,*], Eija Honkavaara [2] and David Luciano Rosalen [3]

[1] Department of Cartography, São Paulo State University UNESP, Presidente Prudente 19060-900, Brazil; erikaasaito@gmail.com (É.A.S.M.); nilton.imai@unesp.br (N.N.I.)
[2] Department of Remote Sensing and Photogrammetry, Finnish Geospatial Research Institute, National Land Survey of Finland, 02150 Espoo, Finland; eija.honkavaara@nls.fi
[3] Department of Engineering and Mathematical Sciences, São Paulo State University, Jaboticabal 14884-900, Brazil; david.rosalen@unesp.br
* Correspondence: a.tommaselli@unesp.br; Tel.: +55-18-32295510

Abstract: Phytosanitary control of crops requires the rapid mapping of diseases to enable management attention. This study aimed to evaluate the potential of vegetation indices for the detection of sugarcane mosaic disease. Spectral indices were applied to hyperspectral images collected by an unmanned aerial vehicle (UAV) to find the areas affected by the mosaic virus in sugarcane. Identifying indices capable of detecting diseased plants in agricultural crops supports data processing and the development of efficient tools. A new index was designed based on spectral regions, which presents higher differences between healthy and mosaic virus-infected leaves to enhance hyperspectral image pixels representing diseased plants. Based on the data generated, we propose the anthocyanin red edge index (AREI) for mosaic virus detection in sugarcane plantations. An index that can adequately identify sugarcane infected by the mosaic virus may incorporate wavelengths associated with variations in leaf pigment concentrations as well as changes in leaf structure. The indices that assessed to detect plants infected with the sugarcane mosaic virus were the normalised difference vegetation index (NDVI), normalised difference vegetation index red edge (NDVI705), new vegetation index (NVI), ARI2 and AREI. The results showed that AREI presented the best performance for the detection of mosaic in sugarcane from UAV images, giving an overall accuracy of 0.94, a kappa coefficient of 0.87, and omission and inclusion errors of 2.86% and 10.52%, respectively. The results show the importance of wavelengths associated with the concentration of chlorophyll and anthocyanin and the position of the red edge for the detection of diseases in sugarcane.

Keywords: vegetation pigments; phytopathology; precision agriculture; crop monitoring; remote sensing; UAV

Citation: Moriya, É.A.S.; Imai, N.N.; Tommaselli, A.M.G.; Honkavaara, E.; Rosalen, D.L. Design of Vegetation Index for Identifying the Mosaic Virus in Sugarcane Plantation: A Brazilian Case Study. *Agronomy* **2023**, *13*, 1542. https://doi.org/10.3390/agronomy13061542

Academic Editors: Silvia Arazuri and Ajit Govind

Received: 28 February 2023
Revised: 9 May 2023
Accepted: 29 May 2023
Published: 1 June 2023

1. Introduction

Agricultural production strategies have changed considerably in recent years due to economic decisions aimed at maximising profits according to environmental guidelines for the safer and more efficient use of chemicals in crops [1]. Identifying areas affected by diseases in plantations is essential in adopting proper management attention.

Phytosanitary problems in sugarcane plantations around the world were firstly identified in 1840 with the rot of sugarcane in Mauritius [2]. In the 1930s, a study was carried out to solve the problems caused by sugarcane gumming disease and mosaics, the first diseases listed in sugarcane cultivation in Brazil [3]. Brazil is the world leader in sugarcane production, and the use of resistant varieties usually controls diseases.

The current scientific efforts have not yet been able to produce a hybrid species resistant to all sugarcane diseases that have characteristics that meet the expectations of agroindustry production [4]. Thus, disease control based on resistant sugarcane varieties

is a complex problem, as varieties susceptible to one or more diseases will always appear in cultivation. Additionally, as agents of diseases are living organisms, they can change, adapt to the environment, become more resistant, and cause damage to the agroindustry.

The development of methodologies that allow for the rapid detection of disease, selecting the correct management focus, and improving pesticide application technologies are fundamental to increasing productivity and bringing advances to the sugarcane industry [5].

In this sense, agricultural crops have been widely characterised, classified, modelled, and mapped using hyperspectral remote sensing data [6]. There are several sensor systems based on RGB, multispectral, hyperspectral, thermal, fluorescence and 3D sensors for the detection of diseases in precision agriculture [7]. Mahlein [7] reviewed the literature about sensing techniques for plant diseases detection and concluded that RGB and hyperspectral sensors demonstrated potential to identify specific diseases. Thus, multi- and hyperspectral images can be used to monitor biochemical and biophysical parameters of vegetation and agricultural crops for stress detection in plants [8]. The information that characterises the crops can be extracted by images represented in "map-driven" data that delimit "management zones", allowing for the realisation of differentiated treatment for different zones [9].

Remote sensing provides a means for identifying and quantifying the differences in the spectral characteristics of surfaces affected by biotic and abiotic stresses and constitutes a tool for monitoring plant health [10]. The spectral reflectance changes in these images are the basis for several vegetation indices that have been developed [10]. Vegetation indices are mathematical models capable of indicating certain characteristics of vegetation [11,12]. The indices are used for various purposes, including the image-based estimation of pigments concentration such as chlorophyll, carotene, and anthocyanin, as well as in the detection of phenological stages, nutritional stress, production estimation, and crop phytosanitary conditions [13–16].

Vegetation indices centred on specific wavelengths contribute to the identification of plant health status; changes in specific regions of the electromagnetic spectrum result from the interaction between incoming radiation and plant pigments, indicating environmental changes, plant senescence phases, and stress occurrence, even when caused by diseases or pests [17,18]. Plant stress and diseases cause a reduction in the concentration of photosynthetic pigments and the formation of necrotic regions, and these factors contribute to changes in the spectral responses of the plant [9].

A deficiency of nutrients in sugarcane, such as nitrogen and potassium, also causes changes to the spectral response of the plant [19]. Bands centred at 410, 430, 720, 754 and 1216 nm have been used to predict the sugarcane nutritional quality, which is highly correlated with the plant's nitrogen concentration [20].

The relationships between anthocyanin, stress and senescence are important indicators for some types of vegetation [21–24]. In addition, the 530 nm is a wavelength that can be an element of an index, as proposed by Gitelson [21], who used the 550 nm wavelength. Chlorophyll a concentration changes when plants are subjected to stress. Many of these indices are based on the change in plant pigment concentration. Changes in the plant structure can occur both in the red edge position and in the NIR region in some situations. Thus, it is clear from these previous studies that vegetation indices may identify plant responses under stress.

When the plant is attacked by phytopathogenic agents, such as fungi, viruses, or bacteria, or undergoes some type of stress, it naturally activates its defence mechanisms, creating physical and chemical barriers. One such mechanism is systemic acquired resistance [25,26]. Viswanathan et al. [27] argued that anthocyanin might be a biochemical factor in systemic resistance induced in sugarcane: when examining red rot, a fungal disease, the researchers verified that the anthocyanin concentration is greater near the inoculation sites of the phytopathogenic agent, suggesting that the plant suffering the attack starts to accumulate more anthocyanin.

Anthocyanins exhibit some properties that act as a defence mechanism in the plant against pathogen attack. These chemicals provide repellence against herbivores and parasites, and their optical properties serve as a visual signal to herbivores, indicating the presence of toxic or unpleasant elements, thus preventing the plant from being attacked [28]. In addition, anthocyanins have been shown to protect plants from pathogenic microorganisms, serving as antiviral, antibacterial and antifungal purposes. Thus, anthocyanin is responsible for disease resistance in several types of agricultural crops [27].

Furthermore, anthocyanin may indicate senescence and stress in some plant species [21]. It can be concluded that, after being infected by the disease, the sugarcane plant will produce a greater amount of anthocyanin. The presence of this pigment can be detected with the ARI2 index using the hyperspectral images.

The main purpose of this work was to design an index for sugarcane mosaic virus identification in remote sensing images. An adequate index to identify sugarcane crops infected by the mosaic virus may incorporate wavelengths associated with variations in leaf pigment concentrations and changes in leaf structure. These indices are needed to design suitable sensors for taking images in the appropriate spectral bands for sugarcane crop monitoring.

Towards this goal, a set of known indices and the one specifically designed in this work, were evaluated. One index was designed based on spectral regions which present higher differences between healthy leaves and those infected with the mosaic virus to enhance hyperspectral image pixels representing sugarcane plants with the disease. These specific spectral regions can be known as sensitive spectral regions. The anthocyanin red edge index (AREI) is proposed for mosaic virus detection. In addition, this work presents a comparative analysis of these designed sugarcane indices with other vegetation indices to enhance the identification of sugarcane plants affected by diseases.

The vegetation indices were designed considering the following steps: spectral analysis of sugarcane leaves, a field study to acquire hyperspectral images using an unmanned aerial vehicle (UAV), processing hyperspectral images, and the application of vegetation index in hyperspectral images.

The contributions of this work were the development of a vegetation index and a solution for monitoring, mapping, and quantifying the damaged sugarcane plants infected with mosaic virus. Although several vegetation indices are available, including spectral indices related to anthocyanin variation, the proposed solution is expected to be more sensitive to inherent variations in the spectral behaviour of sugarcane plants infected with mosaic virus. The solution based on the spectral analysis of healthy and diseased leaves and on the combination of wavelengths sensitive to changes in the plant's spectra, using normalised differences, could be applied in other cases, constituting a contribution to produce other vegetation indices. The design of new vegetation indices is justified by the flexibility when designing new low-cost, lightweight multispectral cameras to detect crop diseases.

General Description of Sugarcane Mosaic Virus (SCMV)

Sugarcane mosaic virus is one of the main viral diseases in sugarcane cultivation in Brazil and is an important virus in Europe and Asia for maise production [29]. From 1922 to 1930, a mosaic epidemic damaged the sugarcane industry in the state of São Paulo (Brazil), causing a 93% reduction in sugarcane production and a 90% reduction in the production of alcohol [4]. The virus is also found in grasses such as maise (*Zea mays* L.), sorghum (*Sorghum bicolour*) and numerous other plants other than aphids. SCMV can be transmitted mechanically or through infected seedlings [4,29].

The mosaic symptoms include chlorosis in a linear arrangement, in the middle or at the base of the leaves, which develops into elongated areas, increasing as the leaf gets older [29]. According to Sanguino [4], the disease is characterised by an alteration in the normal green colour of the leaf, resulting in a lighter or yellowish green colour that forms spots along the whole length of the leaf blade. It may be associated with changes in pigments (chlorophyll

versus carotenoid), resulting in alterations in the visible spectrum. The infection can be accompanied by necrosis of the leaf tissue, associated with changes in near-infrared spectra.

2. Materials and Methodology

The whole experiment methodology can be divided into three parts:

- The first step provided support for the configuration of the airborne hyperspectral imaging system operated onboard a UAV.
- The second step comprised the UAV flight study and the field work that provided support for image acquisition with the camera onboard the UAV. Spectral reference samples were also measured to create a spectral library.
- The last step was the comparison of the proposed indices for sugarcane disease with vegetation indices found in the literature and verifying whether the proposed indices presented an improved potential for the detection of diseases in sugarcane. The conclusions were validated using hyperspectral UAV imagery.

The first step of this study was the spectral analysis of healthy and diseased sugarcane leaves and the index design. The aim of this experimental step was to analyse the spectral differences of sugarcane leaves infected by different pathogenic agents based on spectro-radiometric measurements in the field and laboratory and to identify sensitive spectral regions that can aid in the identification of diseases in sugarcane. Field spectroscopy techniques allow for the extraction of information on plant health and physiology, providing the most detailed spectral characteristics from narrow and continuous spectral bands [30].

Identifying the appropriate spectral regions (in this study, the visible-near infrared range was used) for distinguishing diseases in sugarcane was fundamental for selecting spectral regions to configure the hyperspectral camera and formulate the indices for disease detection in sugarcane crops. Therefore, for the experiments, the camera was configured to reconstruct the spectral reflectance function with a higher level of spectral details in the regions where the diseased leaves can present more significant differences compared to the leaves of healthy plants.

2.1. Study Area

Two study areas were selected to carry out the experiments (sugarcane crop 1 and sugarcane crop 2), located in the state of São Paulo, Brazil.

The sugarcane crop 1 was in the municipality of Euclides da Cunha Paulista (Intermediate geographic region of Presidente Prudente). The planted area of sugarcane in 2021 was the municipality covers 4094 hectares (40.94 km^2) [31]. The coordinates of the study area in the WGS84 system are 22°23′51″ S, 52°31′3.90″ W. The sugarcane crop 2 was in the municipality of Brodowski (Intermediate geographic region of Ribeirão Preto). The planted area of sugarcane in the municipality covers 14,394 hectares (143.94 km^2) [31], and the coordinates of the study area in the WGS84 system are 21°6′54″ S, 47°34′43″ W.

In sugarcane crop 1, there were plants of a mosaic-susceptible variety in an early stage of mosaic infection, and in sugarcane crop 2, there was another sugarcane variety also mosaic-susceptible, in a more advanced stage of mosaic infection.

Due to the field limitations and for safety reasons, a few samples of healthy sugarcane leaves (12 samples) and samples of leaves infected with the mosaic virus of sugarcane (12 samples) were collected from the two study areas (Figure 1). In sugarcane crop 1, two healthy and infected samples were collected (samples 11 and 12, Figure 1a), and in sugarcane crop 2, ten healthy and infected samples were collected (samples 1 to 10, Figure 1b).

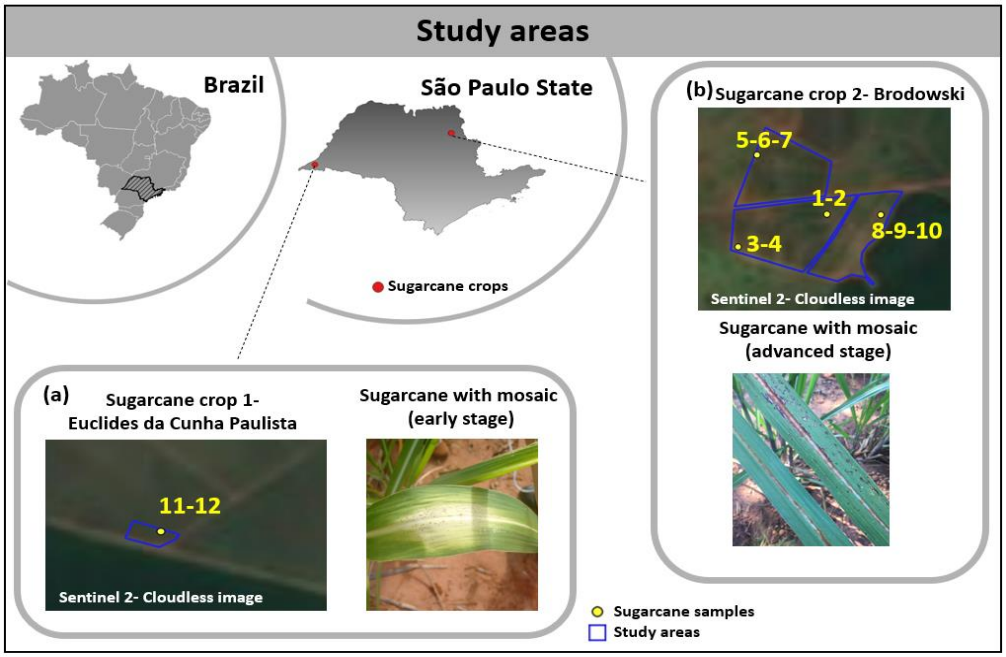

Figure 1. Study areas. (**a**) Sugarcane crop 1, located at Euclides da Cunha Paulista, with an early stage of mosaic infection. (**b**) Sugarcane crop 2 at Brodowski, with an advanced stage of mosaic infection.

Spectroradiometric measurements of healthy and infected sugarcane samples were collected aiming at: (1) producing reference material for the construction of the spectral library used in the radiometric calibration process of the hyperspectral images; and (2) for the identification of the sensitive wavelengths, which enhances differences between healthy and diseased leaves (see details in Section 2.2).

2.2. Index Design for Identifying Sugarcane Mosaic Virus

Figure 2 shows the flowchart of indices design steps, which are detailed in this section.

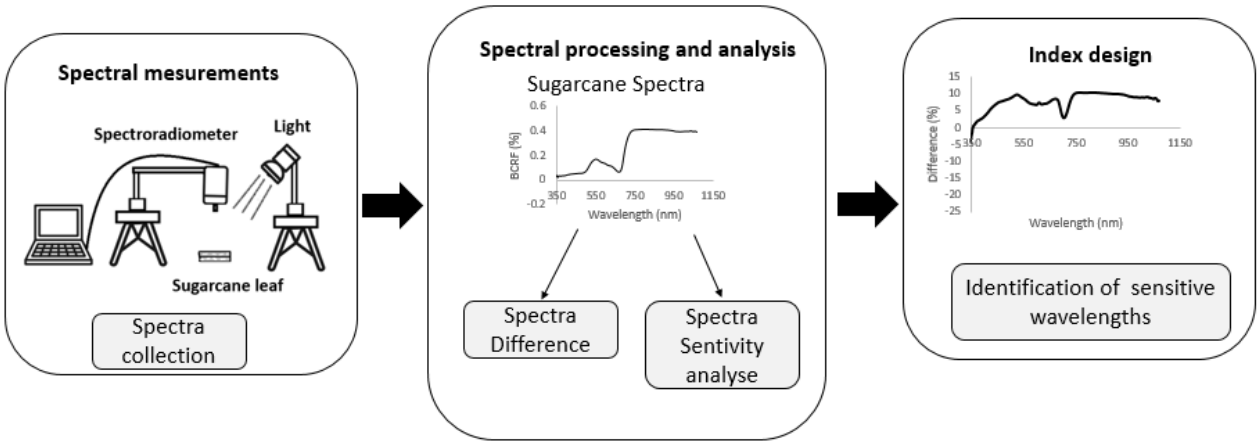

Figure 2. Flowchart of indices design.

Clear differences between the healthy and infested leaves appeared, as can be visualised in Figure 3.

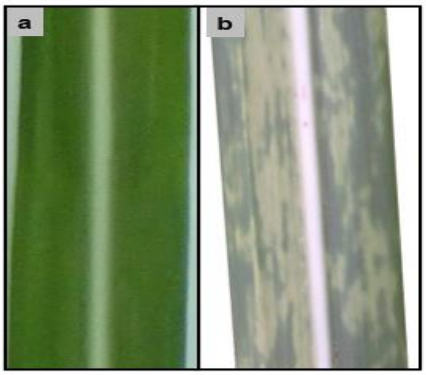

Figure 3. (**a**) Healthy leaf of sugarcane cultivar. (**b**) Leaf infected with mosaic virus.

Spectral measurements were carried out in laboratory conditions. The FieldSpec® UV/NIR spectroradiometer (Analytical Spectral Devices, Boulder, CO, USA) with a FOV of 1° covering a spectral range of 325 nm to 1075 nm was used for spectral measurement. The samples were placed on a black background to avoid transmission of light through the samples and introduce uninterrupted reflections back to the sensor. A Spectralon® board was used to calibrate the spectroradiometer, and a sample of healthy leaves and leaves infected with mosaic was measured.

Ten spectral measurements were made for each sample with the spectroradiometer, and the average spectral data were processed to generate the estimated biconical reflectance factor (BCRF) [32,33].

Spectral processing was carried out to minimise the effects of noise coming from the atmosphere and electronics. A mean filter smoothing with 10 sampled wavelength size was applied to the original BCRF spectrum based on the average set of values within a wavelength window. This processing step provided smoothed spectra.

To identify sensitive spectral regions that could distinguish the healthy and diseased leaf, differences were calculated between the spectra of each kind of leaf, resulting in a spectral difference based on Carter [34]. For the sample of leaves, reflectance differences were calculated by subtracting the mean leaf reflectance of a healthy leaf from that leaf infected by mosaic at each wavelength. The average spectra of the two study cases were used in this analysis. Thus, healthy leaves were compared to the leaves infected by mosaic.

The sensitivity analysis, as detailed by Carter [34], was carried out by dividing the difference between the BCRF spectra by that of a healthy leaf. This procedure was carried out to identify the wavelength in which the BCRF showed a greater pathogenic influence.

Upon completing the spectral analysis stage, the position of the red edge was determined for the leaf samples by calculating the first derivative in the region ranging from 690 nm to 740 nm. The highest derivative representing the red edge position is found within the above wavelength range [35].

Wavelengths that presented the largest differences between the healthy and diseased leaves were selected to be included in the index design.

Indices using the spectral data of the samples of sugarcane leaves were calculated using some of the BCRF identified as sensitive to the presence of pathogens in sugarcane.

2.3. Index Evaluation

Figure 4 shows a flowchart of the index evaluation. The phases included the hyperspectral images collection using a UAV, hyperspectral image processing, application of indices, and analysis of results.

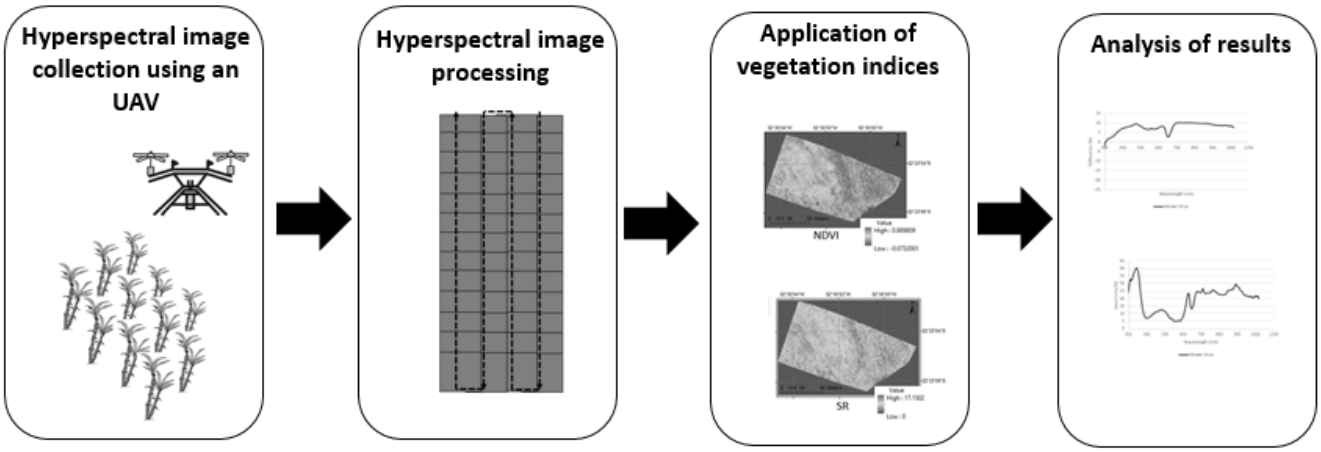

Figure 4. Flowchart of the index's evaluation process. The main steps include hyperspectral image collection using UAV, hyperpesctral image processing, application of vegetation indices and analysis of results.

2.3.1. UAV Image Collection and Processing

Hyperspectral images were acquired with the Rikola hyperspectral camera (Figure 5a) onboard a multirotor UAV model SX8 (Figure 5b) with eight propellers flying over sugarcane crop 1.

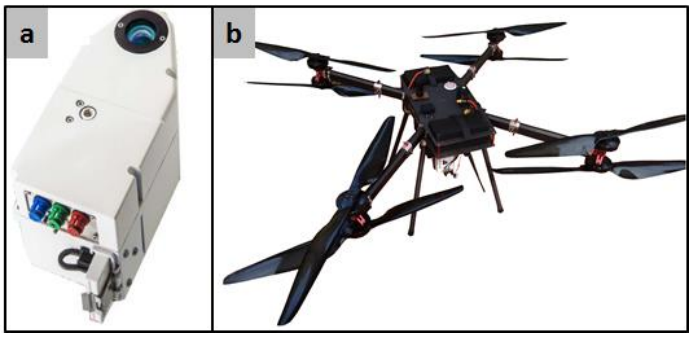

Figure 5. (**a**) Rikola hyperspectral camera, (**b**) multirotor UAV model SX8.

The Rikola model DT-2014 hyperspectral camera with a Fabry–Pérot interferometer (FPI) (Figure 5a) was used to acquire images in the spectral range of 500 to 900 nm and with 25 spectral bands. The camera bands can be set automatically or manually (Rikola Ltd., Oulu, Finland, 2014) [36]. In this case, the bands of the hyperspectral camera were configured based on the spectral analysis of the samples of sugarcane leaf, centred at the following wavelengths (in nanometers) and full widths at half maximum (FWHM): 506.1 (15.6); 520.0 (17.5); 535.5 (16.4); 550.8 (15.2); 564.7 (16.6); 580.1 (15.1); 591.5 (14.7); 605.6 (13.8); 619.5 (14.6); 629.9 (15.9); 650.3 (24.1); 660.3 (24.1); 670.0 (21.7); 680.1 (21.0); 689.6 (21.7); 699.6 (21.9); 709.7 (20.8); 720.0 (20.8); 729.6 (20.8); 740.5 (20.6); 749.7 (19.4); 770.5 (19.4); 790.1 (18.5); 810.2 (17.7); 829.9 (18.6).

The flight height was 160 m, providing images with a ground sample distance (GSD) of approximately 0.11 m. Guo et al. [37] concluded that the optimal spatial resolution aiming for diseases monitoring in crops was 0.1 m. During the field study, targets were installed for the geometric and radiometric correction processes. Ground control points were surveyed with a global navigation satellite system (GNSS) receiver to obtain their accurate coordinates. Radiometric targets were assembled with ethylene vinyl acetate (EVA) in white, grey, and black colours. The EVA targets used for radiometric calibration were measured using the FieldSpec HandHeld® UV/NIR spectroradiometer model ASD,

obtaining their spectra in the range from 325 nm to 1075 nm with a sampling interval of 1.6 nm and FOV of 1° [38].

The hyperspectral image cubes underwent a dark current correction process using a dark target to eliminate noise from the camera electronics. As the images presented spatial displacement between spectral bands, it was also necessary to perform coregistration among these spectral band images. Given the geometric calibration data and the initial coordinates of the exposure stations by GNSS receiver, the spectral bands' images were processed using the Metashape software to compute the exterior orientation parameters with the bundle block adjustment method. A digital surface model (DSM) was produced so that the geometry of the acquisition was retrieved.

The radiometric correction process for the hyperspectral images was performed in the software developed by Honkavaara [39], which considers illumination differences and performs a transformation to a standard acquisition geometry, and consequently minimises the effect of bidirectional reflectance distribution function (BRDF) considering the viewing angle of each pixel in relation to the canopy surface as well as the angle of incidence of the solar radiation based on Walthall Model [39].

The spectral bands' images were orthorectified using exterior and interior orientation parameters, the digital surface model (DSM) with 0.50 m GSD and radiometric correction parameters [40–42].

Using radiometric reference targets, the reflectance calibration of the orthomosaic of hyperspectral images was performed with the empirical line method. Empirical line calibration is based on linear regression, in which the factors of transformation parameters of digital numbers (DNs) into physical values, in this case, hemispherical conical reflectance factors (HCRFs) [43] are calculated. For more details on hyperspectral image cubes processing, see Moriya et al. [44].

2.3.2. Application of Vegetation Indices

Vegetation indices are obtained by radiometric measurements supporting the extraction of information about vegetation characteristics. In this experiment, the ability of some indices to detect diseases was assessed. Table 1 shows the indices applied to the orthomosaic of the hyperspectral images. A histogram contrast stretching was applied to the indices images. Considering the pixels values distribution in this histogram, the minimum and maximum values were adjusted based on the percent clip. The interval slicing produced a pseudo-colour image, and colour values were associated with the thematic classes of the experimental area. The highlighted areas by the indices were compared to the field-checked sample points to verify the potential of vegetation indices to detect diseased areas affected by the mosaic virus.

Table 1. Vegetation indices used in this experiment.

Indices	Formulation	Autor
Simple ratio (SR)	$SR = \frac{p_{nir}}{p_{red}}$	Birth and Macvey, 1968 [45]
NDVI	$NDVI = \frac{\rho_{nir} - \rho_{red}}{\rho_{nir} + \rho_{red}}$	Rouse et al., 1974 [46]
Normalised difference vegetation index red edge (NDVI705)	$NDVI_{705} = \frac{\rho_{750} - \rho_{705}}{\rho_{750} + \rho_{705}}$	Gitelson and Merzlyak, 1994 [47]
Carotenoid reflectance index 1 (CRI1)	$CRI1 = \frac{1}{\rho_{510}} - \frac{1}{\rho_{550}}$	Gitelson et al., 2002 and Gitelson et al. (1997) Gitelson and Merzlyak (1994) [48–50]
Photochemical reflectance index (PRI)	$PRI = \frac{\rho_{531} - \rho_{570}}{\rho_{531} + \rho_{570}}$	Gitelson et al., 2002 [48]
Carotenoid reflectance index 2 (CRI2)	$CRI2 = \frac{1}{\rho_{510}} - \frac{1}{\rho_{700}}$	Gitelson et al., 2002 [48]
Plant senescence reflectance index (PSRI)	$PSRI = \frac{\rho_{680} - \rho_{500}}{\rho_{750}}$	Merzlyak et al., 1999 [50]
Modified chlorophyll absorption ratio index (MCARI)	$MCARI = [(\rho_{700} - \rho_{670}) - 0.2(\rho_{700} - \rho_{550})] * \left(\frac{\rho_{700}}{\rho_{670}}\right)$	Daughtry et al., 2000 [51]

Table 1. *Cont.*

Indices	Formulation	Autor
New vegetation index (NVI)	$NVI = \frac{\rho_{777} - \rho_{747}}{\rho_{673}}$	Gupta et al., 2002 [52]
Transformed chlorophyll absorption reflectance index (TCARI)	$TCARI = 3[(\rho_{700} - \rho_{670}) - 0.2(\rho_{700} - \rho_{550})] * \left(\frac{\rho_{700}}{\rho_{670}}\right)$	Haboudane et al., 2002 [53]
Triangular vegetation index (TVI)	$TVI = 0.5(120(\rho_{nir} - \rho_{green})) - 200(\rho_{red} - \rho_{green})$	Broge and Leblanc, 2000 [54]
Anthocyanin reflectance index 1 (ARI1)	$ARI1 = \frac{1}{\rho_{550}} - \frac{1}{\rho_{700}}$	Gitelson et al., 2001 [55]
Anthocyanin reflectance index 2 (ARI2)	$ARI2 = \rho_{nir}\left(\frac{1}{\rho_{550}} - \frac{1}{\rho_{700}}\right)$	Gitelson et al., 2001 [56]
Optimised soil adjusted vegetation index (OSAVI)	$OSAVI = \frac{1.5*(\rho_{nir} - \rho_{red})}{(\rho_{nir} + \rho_{red} + 0.16)}$	Rondeaux et al., 1996 [55]
Red edge position determination (REP)	$REP = 700 + 40\left[\frac{\rho_{red\ edge} - \rho_{700}}{\rho_{740} - \rho_{700}}\right]$	Clevers, 1994 [56]

2.3.3. Statistical Analysis

To verify the accuracy of the classification results based on different indices, confusion and statistical matrices of the kappa coefficient (Equation (1)) were used [57–59].

$$KAPPA = \frac{\sum_{i=1}^{q} p_{ii} - \sum_{i=1}^{q} p_{i+}p_{+i}}{1 - \sum_{i=1}^{q} p_{i+}p_{+i}} \quad (1)$$

where N is the number of classification pixels in the class q, N_{ij} is the total of lines, and M_i is the total of columns, $p_{ii} = \frac{N_{ij}}{N}$, $p_{i+} = \frac{N_i}{N}$ e $p_{+i} = \frac{M_i}{N}$. $\sum_{i=1}^{q} p_{ii}$ is the main diagonal sum, and $\sum_{i=1}^{q} p_{i+}p_{+i}$ is the sum of the product of the elements of the marginal rows and columns.

Field samples of diseased sugarcane and other classes, including samples of healthy sugarcane, bare soil, and weeds, were used. In the accuracy analysis, 80 sample points selected in the field were used (35 samples of healthy, 35 samples of sugarcane infected with mosaic, and 10 samples of others). Figure 6 shows the spatial distribution of plants inspected in the sugarcane crop. Due to access limitations resulting from the high density of the sugarcane crop, it was only possible to check areas close to the edges.

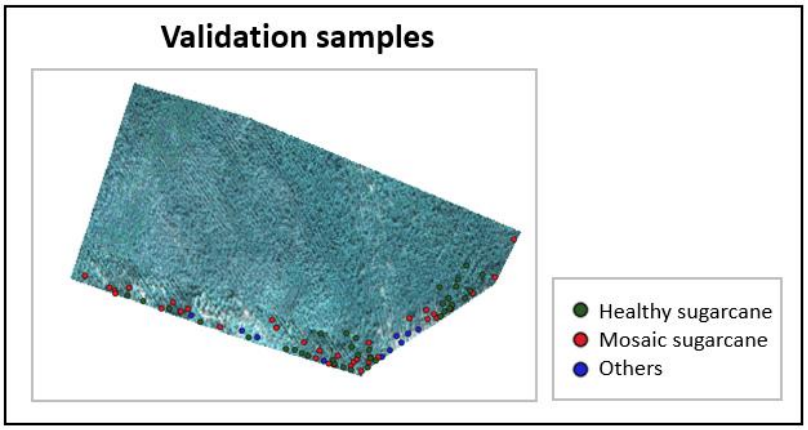

Figure 6. Spatial distribution of validation samples. Green dots represent healthy samples, red dots represent samples infected with mosaic and blue dots represent other types of samples (bare soil/weed).

At the crop, it was also possible to verify the presence of weeds and some areas with failures in the plantation line. Figure 7 shows an example of the plants infected with the mosaic virus. Note that diseased plants were smaller than healthy plants.

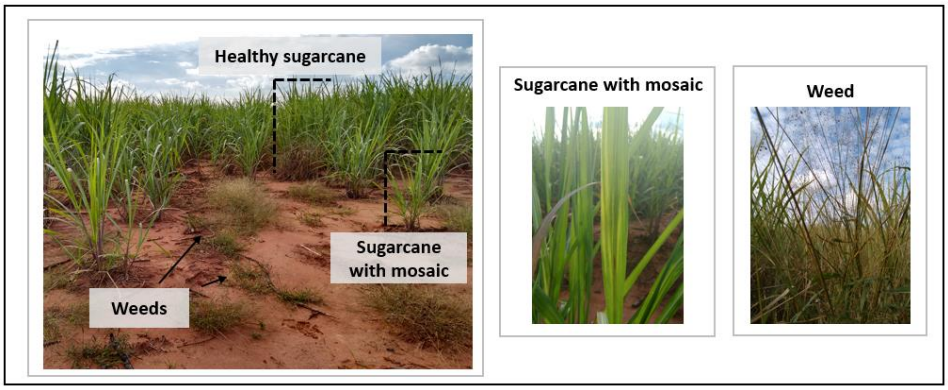

Figure 7. Sugarcane crop infected with mosaic.

3. Results

3.1. Spectral Analysis

The sugarcane spectra measured in the laboratory with a spectroradiometer are depicted in Figure 8. Figure 8a shows the spectra of healthy samples, and Figure 8b the spectra of sugarcane infected with mosaic. As can be seen in Figure 8d, curves attenuate only around the peak of 550 nm (the green light wavelength region). In the case of sugarcane samples infected with mosaics, this attenuation was due to the reduced amount of chlorophyll in the leaves.

The sample infected with mosaic (Figure 8d) was close to the spectral signature of a healthy sugarcane leaf, differing in intensity primarily in the spectral region from 400 nm to 500 nm. Furthermore, there was a decrease in BCRF in the green and red spectral regions.

In the range from 535 to 700 nm, the sample infected with mosaic virus showed similar features, differing only in BCRF intensity. These regions are believed to be significant for differentiating between healthy plants and plants with some sort of alteration, either resulting from a pathogenic origin or due to senescence. In the visible spectral region from 400 nm to 700 nm, the samples infected with mosaic showed lower BCRF values than healthy leaves.

Concerning the near-infrared region, all the samples showed high BCRF values. Among the samples analysed, the mosaic-infected leaf exhibited the lowest values because the measurements were carried out in the laboratory, free of atmospheric influence, which could affect all the other sugarcane leaf samples. Therefore, to detect spectral features in a way to differentiate between diseased and healthy plants, the BCRF difference was calculated by subtracting the BCRF values of a healthy leaf from the values of leaves infected with mosaics (Figure 9a). Overall, there was a similarity in the BCRF difference curves of healthy leaves and those infected with mosaic.

A peak in the region of 530 nm was observed in the BCRF difference curve between the healthy sample and the one infected with mosaics (Figure 9a). Additionally, a dip in the BCRF difference curves between the healthy leaves and those infected with mosaics can be seen near 665 nm. This change in this wavelength appears either as a peak or a dip due to the absorption of chlorophyll a. This feature of maximum absorption of the pigment appears in the region of 660 nm.

For some BCRF difference curves between the healthy leaves and those infected with mosaic, other dips were identified at 705 nm wavelength.

A sensitivity analysis, as described earlier by Carter [33], was carried out to identify the wavelengths at which the BCRF exhibited the greatest relative sensitivity values (Figure 9b). A peak at 530 nm and a dip at 680 nm can be seen in the sensitivity curve for the sample infected with mosaics. There is a plateau in the range from 415 nm to 620 nm and a dip near the 700 nm region, both of which enable the identification of the sugarcane leaf samples infected with mosaics.

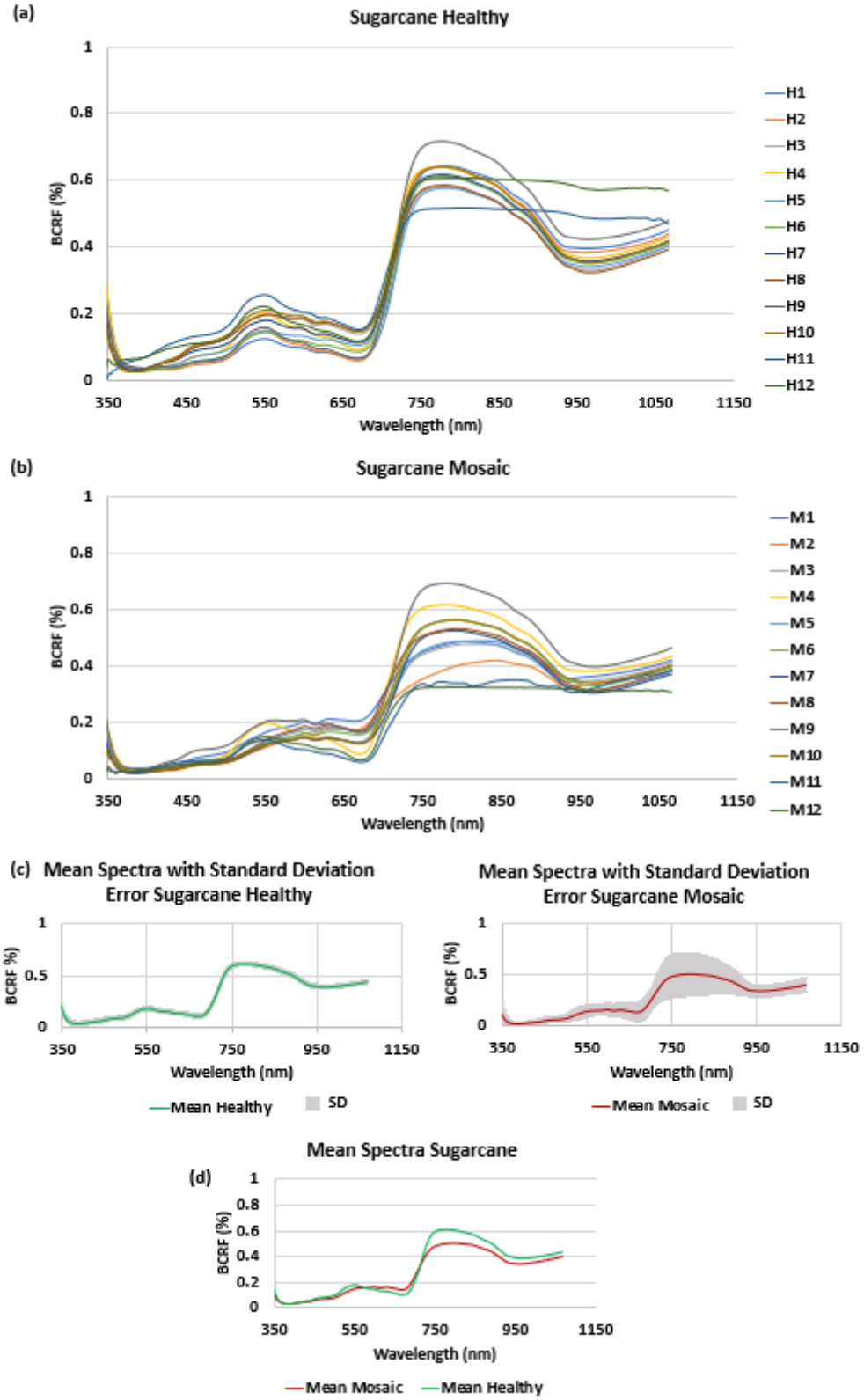

Figure 8. Sugarcane leaves spectra measured using a spectroradiometer. (**a**) Sugarcane healthy spectra (H-healthy). (**b**) Sugarcane with mosaic virus spectra (M-Mosaic). (**c**) Mean spectra with standard deviation error of sugarcane healthy and infected with mosaic virus. (**d**) Mean spectra of healthy sugarcane and infected with mosaic virus.

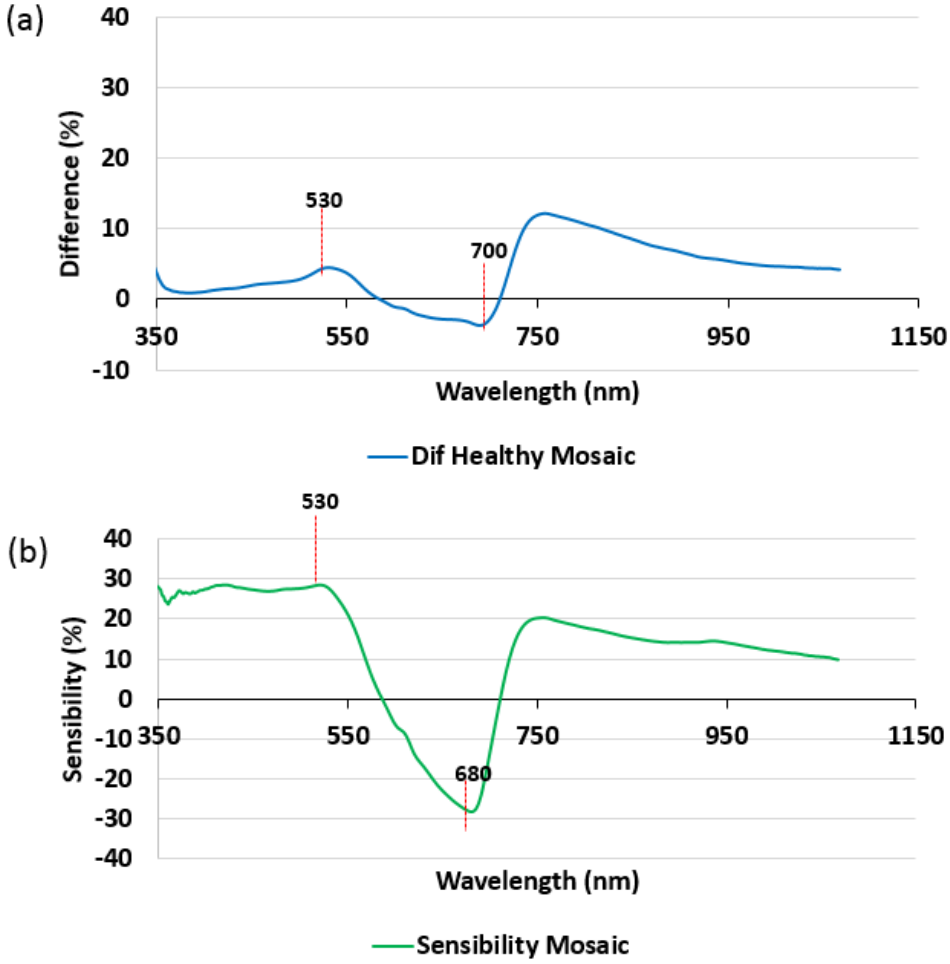

Figure 9. (**a**) Difference between sugarcane leaves infected with the mosaic virus and healthy leaves. (**b**) Sensitivity curves of sugarcane leaves infected with the mosaic virus compared to healthy leaves.

The most relevant features of the spectral analysis of the sugarcane leaves infected with different pathogens can be summarised as follows: A peak in the 530 nm region was observed in the BCRF difference; 700 nm is a significant region because it is located near the red edge position for sugarcane infected with mosaics (705 nm).

Based on this analysis, an index was formulated by combining the HCRF of those wavelengths that are more sensitive to pathogens in sugarcane for mosaic virus detection, and it was proposed as the anthocyanin red edge index (AREI). This index was formulated to be applied and tested with hyperspectral image bands, considering the HCRF measured. In this sense, the wavelengths were chosen from available bands in the hyperspectral image.

This index for sugarcane mosaic detection also comprises the normalised ratio of two wavelengths, 530 nm and 700 nm. In this case, the 530 nm wavelength was chosen because it presented a prominent peak in the spectral analysis of the HCRF difference between healthy leaves and those infected with mosaics. The 530 nm wavelength was selected because the highest sensitivity in the spectral analysis was achieved near this region (531 nm). The wavelength 700 nm was used because it is close to the red edge region (705 nm), as it was identified for sugarcane infected with mosaics in the spectral analysis.

$$Anthocyanin\ Red\ Edge\ Index\ (AREI) = \frac{HCRF_{700} - HCRF_{530}}{HCRF_{700} + HCRF_{530}} \quad (2)$$

3.2. Application of Indices in Hyperspectral Images

Figure 10 presents the resulting vegetation indices maps obtained from the hyperspectral mosaics. For visual analysis, infected areas are highlighted in yellow. The indices that most emphasised the regions infected with sugarcane mosaic (Figure 10) were the NDVI, NDVI705, NVI, ARI2 and AREI. The PRI, CRI1 and CRI2 indices emphasised the hyperspectral image noise, and the MCARI, TCARI and REP indices did not detect the mosaic in sugarcane orthomosaics. The AREI index had a better performance in identifying the regions affected by mosaic since it is based on the wavelengths sensitive to the presence of this virus.

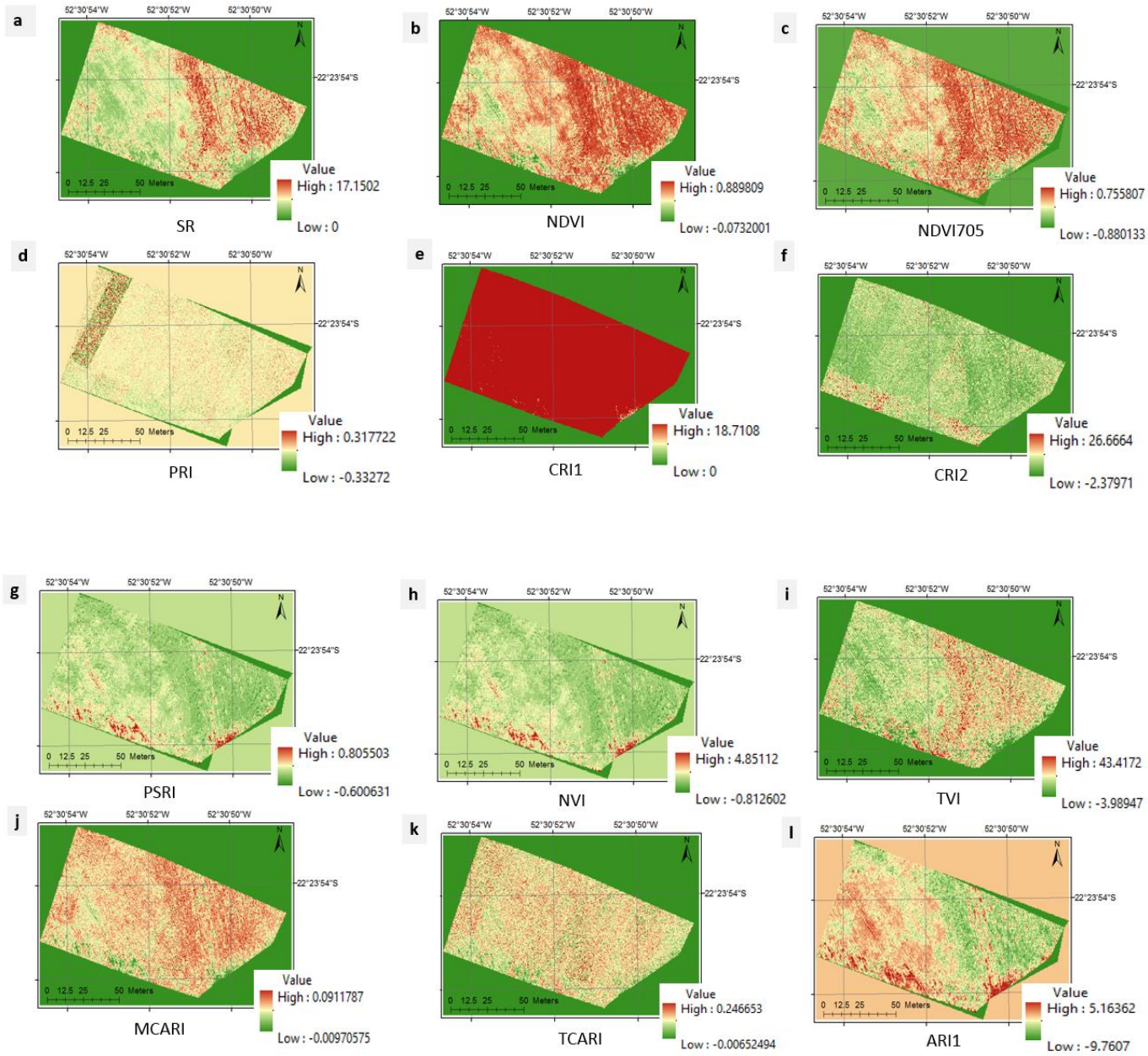

Figure 10. *Cont.*

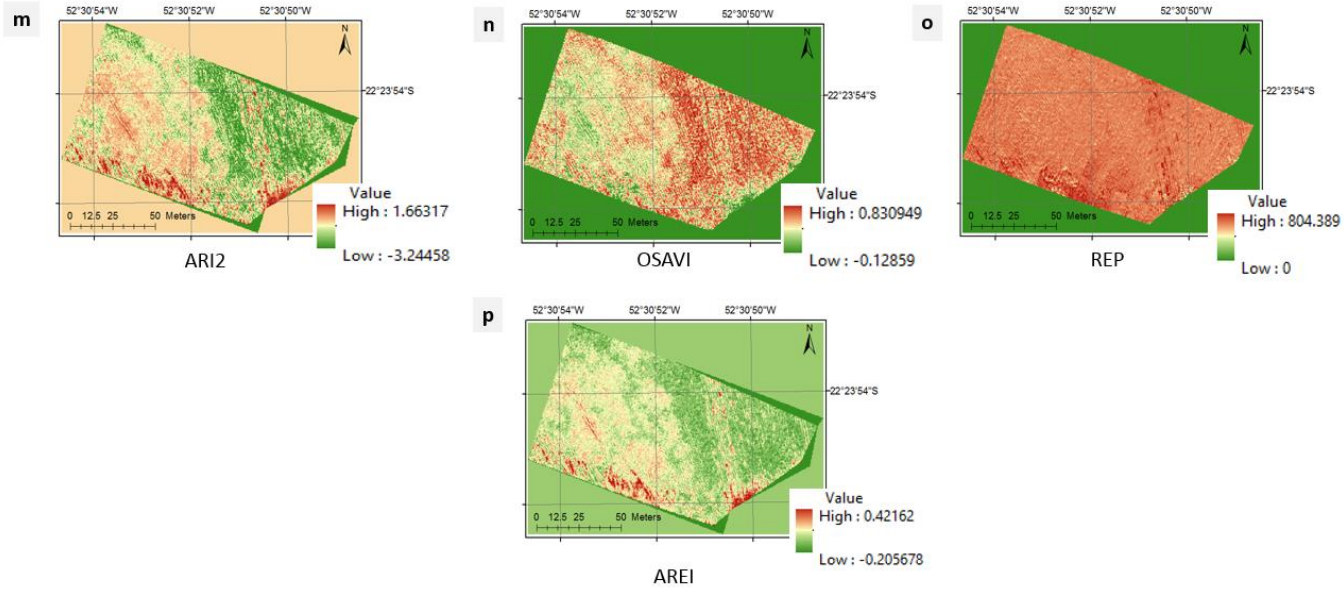

Figure 10. Results of classification by density slicing of vegetation indices for areas of sugarcane infected with mosaic. (**a**) SR, (**b**) NDVI, (**c**) NDVI705, (**d**) PRI, (**e**) CRI1, (**f**) CRI2, (**g**) PSRI, (**h**) NVI, (**i**) TVI, (**j**) MCARI, (**k**) TCARI, (**l**) ARI1, (**m**) ARI2, (**n**) OSAVI, (**o**) REP, (**p**) AREI.

For each classified index map, the global accuracy (Congalton et al. [60]; Landis and Koch [61]) of the mapping and the kappa coefficient were calculated (Table 2). The highest kappa coefficient values were obtained for the AREI (a global accuracy of 0.94 and kappa coefficient of 0.87), ARI2 (a global accuracy of 0.85 and kappa coefficient of 0.69), NVI (a global accuracy of 0.78 and kappa coefficient of 0.56) and NDVI705 (a global accuracy of 0.71 and kappa coefficient of 0.41).

Table 2. Global accuracy and kappa coefficients of vegetation index result for mosaic-infected sugarcane areas.

Indices	Global Accuracy	Kappa	Omission Error of Sugarcane with Mosaic (%)	Inclusion Error of Other Classes (%)
SR	0.63	0.27	20.00	45.09
NDVI	0.70	0.35	60.00	17.64
NDVI705	0.71	0.41	34.29	32.35
CRI1	0.58	0.13	54.28	48.38
PRI	0.69	0.35	42.85	33.33
CRI2	0.49	−0.06	68.57	60.71
PSRI	0.46	−0.09	60.00	61.11
NVI	0.78	0.56	8.57	31.91
TVI	0.66	0.33	28.57	40.47
MCARI	0.63	0.22	54.29	40.74
TCARI	0.45	−0.19	42.85	41.17
ARI1	0.69	0.40	5.71	41.07
ARI2	0.85	0.69	20.00	15.15
OSAVI	0.68	0.35	28.57	39.02
REP	0.50	0.09	5.71	53.52
AREI	0.94	0.87	2.86	10.52

Even presenting an overall accuracy value of 0.69, the classification image based on PRI was considered noisy. Similarly, CRI1, MCARI, TCARI, and REP indices provided poor results.

Considering the omission and inclusion errors, the AREI provided the best performance, with 2.86% and 10.52%, respectively. Analysing the kappa coefficient of the indices,

the ARI2 had good and consistent results, with omission and inclusion errors of 20.0% and 15.15%.

4. Discussions

The sugarcane spectra showed features typical of vegetation. The general characteristic of the spectral curve of the sugarcane canopy was a low reflectance in the visible light region (400–700 nm), peaking between 550 nm and 560 nm, the wavelength regions of green light [62]. Hence, reflectivity and transmittance are observed to be low due to the absorption of pigments in the sugarcane leaves [63]. In the visible region, the high absorption of electromagnetic energy is due to the presence of photosynthetic pigments [62,64]. The three main classes of plant pigments are chlorophylls, carotenoids, and phycobilins [65]. In the case of sugarcane leaves, the pigments found are those typical of green leaves and include chlorophyll a and b, carotenoids, xanthophylls and lutein [65].

The spectral features of diseased and healthy sugarcane leaves differed, differing in intensity primarily in the spectral region from 400 nm to 500 nm, and there was a decrease in BCRF in the green and red spectral regions in the infected leaves. Krezhova et al. [66] noted similar behaviour when analysing tobacco leaves inoculated with TSWV (tomato spotted wilt virus) and found that even a sample leaf in the asymptomatic stage exhibited this behaviour.

Jones et al. [67] analysed the spectral features of tomato leaves infected with the bacterial disease *Xanthomonas perforans*, and noted higher absorption in the light blue region (450–495 nm) and the red-light region (620–750 nm) and reduced absorption in the green light region (495–570 nm), with a minimum absorption of approximately 550 nm.

Analysing vine leaves infected with Grapevine leafroll disease caused by virus_3, Naidu et al. [16] noted differences between diseased and healthy leaves mainly at the green light peak (550 nm), the near-infrared (900 nm) and in the mid-infrared (1600 nm to 2200 nm). Naidu et al. [16] noted that maximum differences at 550 nm and 680 nm indicate a change in the absorption of chlorophyll by the infected leaves. Furthermore, wavelengths near 530 nm represent the second peak of maximum fluorescence in the green region of vegetation [68,69].

Additionally, the spectral region near 550 nm can indicate the absorption of carotenoid pigments. Another characteristic feature of carotenoid absorption is noticeable in the BCRF difference curves at 510 nm. Carotenoids, yellow, orange, and red pigments [70], contribute to the energy supply to the photosynthetic system [71]. The plant's natural colour can be altered when physiological changes occur, caused by a deficiency in nutrients or water, or when the plant is attacked by a pathogen that destroys its cells, causing necrosis [72]. Thus, when a plant is stressed or in the senescence stage, chlorophyll pigments can disappear, enabling other pigments, such as carotene, to become apparent [13].

In addition, Puchades [73] carried out a genetic and symptomatic characterisation of the sugarcane mosaic virus and observed differences in pigments concentrations such as chlorophyll a, chlorophyll b and total carotenoids, which were correlated with the percentage of mosaic virus infection. The results from our study also showed that the presence of the virus causes changes in the spectra of sugarcane.

The slant at 665 nm was observed in all spectra difference curves of the sugarcane leaf samples analysed, indicating a possible relationship with the absorption of chlorophyll at 660 nm [65,74].

Several vegetation indices are found in the literature using 700 nm wavelengths in their formulations [49,52,56]. This wavelength is associated with the absorption of chlorophyll a [65,74]. At a closer wavelength (665 nm), the spectra difference appeared as a valley in all samples analysed in the spectral analysis stage.

Gamon et al. [75,76] used a wavelength of 531 nm to formulate the photochemical reflectance index (PRI). Even though the overall accuracy value of the PRI was 0.69, the resulting mosaic virus classification image was considered noisy and of poor quality, with omission and inclusion errors of 42.85% and 33.33%, respectively.

The PSRI is an indicator of stress, senescence, and fruit maturation processes, as it is associated with carotene pigment (Merzlyak et al. [50]); in the case of this experiment, it had an accuracy of 0.46 to detect mosaic virus. ARI1 and ARI2 indices related to content anthocyanin pigment [55] obtained accuracies of 0.69 and 0.85, respectively.

The NVI was developed to improve the biomass monitoring capacity of the NDVI [53], and the NDVI705 is a modification of the NDVI based on the red edge developed by Gitelson and Merzlyak [47], which is correlated with the presence of chlorophyll and deciduous vegetation. It performed quite well, providing an overall accuracy of 0.78, a Kappa coefficient of 0.56, and omission and inclusion errors of 8.57% and 31.91%, respectively.

The ARI2 index presented an interesting performance for detecting diseases in sugarcane for mosaic virus detection. This index is used to estimate the concentrations of anthocyanin [55], a pigment present in plants and fruits, which is responsible for the combination of red and blue colours. In the case of sugarcane leaves, the found pigments, such as chlorophyll a and b, carotenoids and anthocyanin, are typical of green leaves [27,77,78]. It provided an overall accuracy of 0.85 and kappa of 0.69, and omission and inclusion errors of 20.00% and 15.15%. This performance was substantial according to the standards of Landis and Koch [61], indicating that ARI2 may be a potential index for the detection of mosaic virus in sugarcane.

This study developed a new index AREI, which presented a high potential for the detection of mosaics in sugarcane. This index was developed based on a spectral analysis performed to identify disease-sensitive wavelengths in sugarcane, which was essential for identifying combinations of wavelengths for the formulation of the index.

The AREI considers the 530 nm wavelength associated with anthocyanin absorption [22]. This wavelength is used in laboratory measurements of anthocyanin concentrations using spectrophotometry [23]. Van den Berg and Perkins [24] proposed using the ratio of 530 nm and 940 nm wavelengths to obtain the anthocyanin content by the anthocyanin content index (ACI). This information further reinforces the importance of anthocyanin pigments concerning the stress caused by pathogenic agents in sugarcane.

The wavelength 700 nm is associated with the red edge position in sugarcane infected with mosaic and combined with the wavelength of 530 nm, allowed for the detection of mosaic in sugarcane. It provided the best performance, with an overall accuracy of 0.94 and kappa of 0.87, and omission and inclusion errors of 2.86% and 10.52%.

The results obtained from this evaluation constitute a significant step towards detecting diseases in sugarcane. The identification of indices capable of detecting diseased plants is important because it facilitates data processing, allowing suitable management when aiming to quantify the damaged area. In this case, study, approximately 40% of the crop area was affected by the disease.

In addition, these results enable the use of sensors designed for imaging in the appropriate spectral bands for monitoring the sugarcane crop. The contribution of this work to agriculture relies on the specification of appropriate indices for monitoring an important disease in sugarcane crops and in the production of maps in support of the georeferenced crop management.

5. Conclusions

This article presented a methodology for formulating specific spectral indices for disease detection in sugarcane. In the first stage of the research, wavelengths sensitive to pathogens in sugarcane were identified based on spectroradiometric measurements. From these results, the bands of a hyperspectral sensor were configured, and an index for detecting the mosaic virus in sugarcane was proposed. Hyperspectral images were acquired from a sugarcane field infected with this mosaic virus via a UAV, and the processed orthomosaics were used to compute vegetation indices found in the literature and the index proposed in this work, the AREI.

The indices that contributed to the detection of the regions infected with sugarcane mosaic were NDVI, NDVI705, NVI and ARI2. However, AR1 and ARI2 stood out the

most among the indices found in the literature. The study shows that all of the indices commonly used in evaluations of the health of agricultural crops were not accurate in detecting phytosanitary problems. Among the indices analysed, those presenting the highest accuracy were the AREI, which exhibits high potential for the detection of mosaic in sugarcane, based on digital image analysis. In some cases, a specific index has to be formulated to solve a phytosanitary problem. For example, the AREI, showed greater accuracy in detecting phytosanitary problems in sugarcane crops.

The results show the importance of wavelengths associated with the concentration of chlorophyll and anthocyanin and the position of the red edge for the detection of diseases in sugarcane. However, it is necessary to carry out more tests to verify whether the variations in the phenological stage and sugarcane variety, among other features, may influence the spectral behaviour of sugarcane and whether the development of other indices is necessary. Another suggestion would be to test AREI with multispectral aerial or satellite images.

Author Contributions: Conceptualization, É.A.S.M., N.N.I., A.M.G.T., E.H. and D.L.R.; methodology, É.A.S.M., N.N.I., A.M.G.T., E.H. and D.L.R.; software, É.A.S.M., N.N.I., A.M.G.T. and E.H.; validation, É.A.S.M., N.N.I., A.M.G.T. and D.L.R.; formal analysis, É.A.S.M., N.N.I., A.M.G.T., E.H. and D.L.R.; investigation, É.A.S.M., N.N.I., A.M.G.T., E.H. and D.L.R.; resources, N.N.I., A.M.G.T., E.H. and D.L.R.; data curation, É.A.S.M., N.N.I., A.M.G.T. and D.L.R.; writing—original draft preparation, É.A.S.M., N.N.I., A.M.G.T. and E.H.; writing—review and editing, É.A.S.M., N.N.I., A.M.G.T., E.H. and D.L.R.; visualization, É.A.S.M., N.N.I., A.M.G.T., E.H. and D.L.R.; supervision, É.A.S.M., N.N.I. and A.M.G.T.; project administration, N.N.I. and A.M.G.T.; funding acquisition, N.N.I. and A.M.G.T. All authors have read and agreed to the published version of the manuscript.

Funding: This research was funded by São Paulo Research Foundation (FAPESP) (grants 2013/50426-4 and 2021/06029-7), National Council for Scientific and Technological Development (CNPq—grants n. 303670/2018-5, 151486/2018-2 and 308747/2021-6), Brazilian Federal Agency for Support and Evaluation of Graduate Education (CAPES) for a Doctoral Scholarship and Mobility (Program Capes-PrInt 88881.310314/2018-01) and Foundation for Unesp development (Fundunesp-2530/2016).

Data Availability Statement: Not applicable.

Conflicts of Interest: The authors declare no conflict of interest.

References

1. Bassoi, L.H.; Miele, A.; Reisser, C., Jr.; Gebler, L.; Flores, C.A.; Alba, J.M.F.; Grego, C.R.; Terra, V.S.S.; Timm, L.C.; Nascimento, P.S. Agricultura de precisão em fruticultura. In *Agricultura de Precisão Resultados de um Novo Olhar*; Bernardi, A.C.C., Naime, J.M., Resende, A.V., Bassoi, L.H., Inamasu, R.Y., Eds.; Embrapa Instrumentação: Brasília, Brazil, 2014; p. 596, ISBN 978-85-7035-352-8. (In Portuguese)
2. Bailey, R.A. Diseases. In *World Agriculture Series*, 2nd ed.; Sugarcane, J.G., Ed.; Blackwell Science: Oxford, UK, 2004; p. 216, ISBN 0-632-05476-X.
3. IAC, Instituto Agronômico de Campinas. *Ciência da Terra: O Instituto Agronômico e a Pesquisa em Benefício da Qualidade de Vida*; Moreira, A.C., Castro, O.M., Eds.; Instituto Agronômico: Campinas, Brazil, 2008; p. 160. (In Portuguese)
4. Sanguino, A. *As Principais Doenças da Cana-de-Açúcar*; Curso à distância Tópicos da Cultura de cana-de-açúcar; IAC: Ribeirão Preto, Brazil, 2012; p. 22. (In Portuguese)
5. Mentem, J.O. Cana de Açúcar: Apenas 5 Fungicidas Combatem a Ferrugem Alaranjada. Portal Agrolink. 2015. Available online: http://www.agrolink.com.br/agrolinkfito/noticia/cana-de-acucar{-}{-}apenas-5-fungicidas-combatem-ferrugem-alaranjada_221889.html (accessed on 1 September 2015). (In Portuguese)
6. Thenkabail, P.S.; Lyon, J.G.; Huete, A. Advances in hyperspectral remote sensing of vegetation and agricultural croplands. In *Hyperspectral Remote Sensing of Vegetation*; Thenkabail, P.S., Lyon, J.G., Huete, A., Eds.; CRC Press Taylor & Francis Group: New York, NY, USA, 2012; pp. 3–35.
7. Mahlein, A.K. Plant disease detection by imaging sensors—Parallels and specific demands for Precision Agriculture and plant phenotyping. *Plant Dis.* **2016**, *100*, 241–251. [CrossRef]
8. Gosh, P.P.; Banik, P.; Patel, N.; Pal, D.J. Vegetation stress detection with hyperspectral Remote Sensing for a winning agribusiness. *Internat. J. Bus. Analyst. Intell.* **2013**, *1*, 13–21.
9. Yao, H.; Tang, L.; Tian, L.; Brown, R.L.; Bhatnagar, D.; Cleveland, T.E. Using hyperspectral data in precision farming applications. In *Hyperspectral Remote Sensing of Vegetation*; Thenkabail, P.S., Lyon, J.G., Huete, A., Eds.; CRC Press Taylor & Francis Group: New York, NY, USA, 2012; pp. 309–327.

10. Mirik, M.; Ansley, R.J.; Price, J.A.; Workneh, F.; Rush, C. Remote monitoring of wheat streak mosaic progression using sub-pixel classification of Landsat 5 TM imagery for site specific disease management in winter wheat. *Adv. Remote Sens.* **2013**, *2*, 16–28. [CrossRef]
11. Elvidge, C.D.; Chen, Z. Comparison of broad-band and narrow-band red and near-infrared vegetation indices. *Remote Sens. Environ.* **1995**, *54*, 38–48. [CrossRef]
12. Jensen, J.R. *Remote Sensing of the Environment: An Earth Resource Perspective*; Prentice-Hall: Saddle River, NJ, USA, 2007; ISBN 13 978-0131889507.
13. Jackson, R.D.; Huete, A.R. Interpreting vegetation indices. *Prev. Vet. Med.* **1991**, *11*, 185–200. [CrossRef]
14. Naidu, R.A.; Perry, E.M.; Pierce, F.; Mekuria, T. The potential of spectral reflectance technique for the detection of Grapevine leafroll-associated vírus-3 in two red-verried wine grape cultivars. *Comp. Electron. Agric.* **2009**, *66*, 38–45. [CrossRef]
15. Ashourloo, D.; Mobasheri, M.R.; Huete, A. Developing two spectral disease indices for detection of wheat leaf rust (*Pucciniatriticina*). *Remote Sens.* **2014**, *6*, 4723–4740. [CrossRef]
16. Singh, S.K.; Dutta, S.; Dharaiya, N.A. Efficiency of remote sensing indices in crop biotic stress assessment. *Int. J. Life Sci. Educ. Res.* **2013**, *1*, 100–104.
17. Gitelson, A.A.; Merzlyak, M.N. Signature analysis of leaf reflectance spectra: Algorithm development for remote sensing of chlorophyll. *J. Plant Physiol.* **1996**, *148*, 494–500. [CrossRef]
18. Malthus, T.J.; Madeira, A.C. High resolution spectroradiometry: Spectral reflectance of Field bean leaves infected by *Botrytis fabae*. *Remote Sens. Environ.* **1993**, *45*, 107–116. [CrossRef]
19. Jackson, R.D.; Jones, C.A.; Uehara, G.; Santo, L.T. Remote detection of nutrient and water deficiencies in sugarcane under variable cloudiness. *Remote Sen. Environ.* **1980**, *11*, 327–331. [CrossRef]
20. Miphokasap, P.; Honda, K.; Vaiphasa, C.; Souris, M.; Nagai, M. Estimating canopy concentration in sugarcane using Field imaging spectroscopy. *Remote Sens.* **2012**, *4*, 1651–1670. [CrossRef]
21. Gitelson, A.A.; Merzlyak, M.N.; Zur, Y.; Stark, R.; Gritz, U. Non-desctrutive and remote sensing techniques, for estimation of vegetation status. In Proceedings of the Third European Conference on Precision Agriculture, Montpellier, France, 18–20 June 2001; Volume 1, pp. 205–210.
22. Pirie, A.; Mullins, M.G. Changes in anthocyanin and phenolics content of grapevine leaf and fruits tissues treated with sucrose, nitrate and abscisic acid. *Plant Physiol.* **1976**, *58*, 468–472. [CrossRef] [PubMed]
23. Nakata, M.; Ohme-Takagi, M. Quantification of anthocyanin content. *Bio-Protocol* **2014**, *4*, 3. [CrossRef]
24. Van Den Berg, A.K. Nondestructive estimation of anthocyanin content in autumn sugar maple leaves. *HortScience* **2005**, *40*, 685–686. [CrossRef]
25. Guest, D.; Brown, J. Plant defences against pathogens. In *Plant Pathogens and Plant Diseases*; Brown, J.F., Ogle, J.H., Eds.; Rockvale Publications: Armidale, Australia, 1997; pp. 263–286.
26. Fernandes, C.F.; Vieria Júnior, J.R.; Silva, D.S.G.; Reis, N.D.; Antunes Júnior, H. *Mecanismo de Defesa de Plantas Contra o Ataque de Agentes Fitopatogênicos*; Embrapa Rondônia: Porto Velho, Brazil, 2009; p. 14. (In Portuguese)
27. Viswanathan, R.; Mohanraj, D.; Padmanaban, P. Possible involvement of anthocyanin compounds in resistance of sugarcane against red rot. *Indian Phytopathol.* **2000**, *53*, 311–313.
28. Lev-Yaudan, S.; Gould, K.S. Role of anthocyanins in plant defense. In *Anthocyanins: Biosynthesis, Functions and Applications*; Winefield, C., Davies, K., Gould, K., Eds.; Springer: New York, NY, USA, 2009; pp. 22–28.
29. Gonçalves, M.C. Doenças causadas por vírus. In *Cana-de-Açúcar*; Dinardo-Miranda, L.L., Vasconcelos, A.C.M., Landell, M.G.A., Eds.; Instituto Agronômico: Campinas, Brazil, 2010; p. 882, ISBN 978-85-855564-17-9. (In Portuguese)
30. Middleton, E.M.; Huemmrinch, K.F.; Cheng, Y.-B.; Margolis, H.A. Spectral bioindicators of photosynthetic efficiency and vegetation stress. In *Hyperspectral Remote Sensing of Vegetation*; Thekabail, P.S., Lyon, J.G., Huete, A., Eds.; CRC Press: New York, NY, USA, 2011; pp. 265–288, ISBN 978-1-4398-4598-4538-7.
31. Instituto Brasileiro de Geografia e Estatística (IBGE). Produção Agrícola Municipal. 2021. Available online: https://www.ibge.gov.br/estatisticas/economicas/agricultura-e-pecuaria/9117-producao-agricola-municipal-culturas-temporarias-e-permanentes.html?=&t=resultados (accessed on 1 July 2021). (In Portuguese)
32. Milton, E.J. Principles of field spectroscopy. *Int. J. Remote Sens.* **1987**, *8*, 1807–1827. [CrossRef]
33. Schaepman-Strub, G.; Schaepman, M.E.; Painter, T.H.; Dangel, S.; Martonchik, J.V. Reflectance quantities in optical remote sensing—Definitions and case studies. *Remote Sens. Environ.* **2006**, *103*, 27–42. [CrossRef]
34. Carter, G.A. Primary and secondary effects of water content on the spectral reflectance of leaves. *Am. J. Bot.* **1991**, *78*, 916–924. [CrossRef]
35. Curran, P.; Windham, W.; Gholz, H. Exploring the relationship between reflectance red edge and chlorophyll concentration in slash pine leaves. *Tree Physiol.* **1990**, *7*, 33–48. [CrossRef]
36. Rikola, L.T.D. *Rikola Hyperspectral Imager Manual*; Rikola Ltd.: Oulo, Finland, 2014; Volume 37.
37. Guo, A.; Huang, W.; Dong, Y.; Ye, H.; Ma, H.; Liu, B.; Wu, W.; Ruan, C.; Geng, Y. Wheat yellow rust detection using UAV-Based hyperspectral technology. *Remote Sens.* **2020**, *13*, 123. [CrossRef]
38. ASD. FieldSpec UV/VNIR: HandHeld Spectroradiometer. In *User's Guide*; Analytical Spectral Devices, Inc.: Boulder, USA, 2003; p. 72.

39. Honkavaara, E.; Saari, H.; Kaivosoja, J.; Pölönen, I.; Hakala, T.; Litkey, P.; Mäkynen, J.; Pesonen, L. Processing and assessment of spectrometric, stereoscopic imagery collected using a lightweight UAV Spectral Camera for Precision Agric. *Remote Sens.* **2013**, *5*, 5006–5039. [CrossRef]
40. Walthall, C.L.; Norman, J.M.; Welles, J.M.; Campbell, G.; Blad, B.L. Simple equation to approximate the bidirectional reflectance from vegetative canopies and bare soil surfaces. *Appl. Opt.* **1985**, *24*, 383–387. [CrossRef]
41. Hakala, T.; Honkavaara, E.; Saari, H.; Mäkynen, J.; Kaivosoja, J.; Pesonen, L.; Pölönen, I. Spectral imaging from UAVS varying illumination conditions. *Intern. Arch. Photogram. Remote Sens. Spat. Inf. Sci.* **2013**, *XL-1/W2*, 189–194. [CrossRef]
42. Honkavaara, E.; Kaivosoja, J.; Mäkynen, J.; Pellikka, I.; Pesonen, L.; Saari, H.; Salo, H.; Hakala, T.; Markelin, L.; Rosnell, T. Hyperspectral reflectance signatures and point clouds for precision agriculture by light weight UAV imaging system. *ISPRS Ann. Photogramm. Remote Sens. Spat. Sci* **2012**, *I-7*, 353–358. [CrossRef]
43. Sahoo, R.N.; Pargal, S.; Pradhan, S.; Krishna, G.; Gupta, V.K. *Processing of Hyperspectral Remote Sensing Data*; Division of Agriculture Physics, Indian Agriculture Research Institute: New Delhi, India, 2013; p. 72.
44. Moriya, É.A.S.; Imai, N.N.; Tommaselli, A.M.G.; Miyoshi, G.T. Mapping Mosaic Virus in Sugarcane Based on Hyperspectral Images. *IEEE J. Sel. Top. Appl. Earth Obs. Remote Sens.* **2016**, *10*, 740–748. [CrossRef]
45. Birth, G.S.; Mcvey, G. Measuring the colour of growing turf with a reflectance spectrophotometer. *Agron. J.* **1968**, *60*, 640–643. [CrossRef]
46. Rouse, J.W.; Haas, R.H.; Schell, J.A.; Deering, D.W. Monitoring vegetation systems in the great plains with ERTS. In Proceedings of the Third Earth Resources Technology Satellite-1 Symposium, Washington, DC, USA, 10–14 December 1973; NASA SP-351. NASA: Greenbelt, MD, USA, 1974; pp. 3010–3017.
47. Gitelson, A.A.; Merzlayak, M.N. Spectral Reflectance changes associated with autumn senescence of Aesculus hippocastanum L. and Acer platanoides L. Leaves. Spectral features and relation to chlorophyll estimation. *J. Plant Physiol.* **1994**, *143*, 286–292. [CrossRef]
48. Gitelson, A.A.; Zur, Y.; Chivkunova, O.B.; Merzlyak, M.N. Assessing carotenoid contend in plant leaves with reflectance spectroscopy. *Photochem. Photobiol.* **2002**, *75*, 272–281. [CrossRef]
49. Gitelson, A.A.; Merzlyak, M.N. Remote estimation of chlorophyll content in higher plant leaves. *Int. J. Remote Sens.* **1997**, *18*, 2691–2697. [CrossRef]
50. Merzlyak, M.N.; Gitelson, A.A.; Chivkunova, O.B.; Rakitin, V.Y. Non-destructive optical detection of pigment changes during leaf senescence and fruit ripening. *Physiol. Plant.* **1999**, *106*, 135–141. [CrossRef]
51. Daughtry, C.S.T.; Walthall, C.L.; Kim, M.S.; Colstoun, E.B.; Mcmurtrey, J.E., III. Estimating corn leaf chlorophyll concentration from leaf and canopy reflectance. *Remote Sens. Environ.* **2000**, *74*, 229–239. [CrossRef]
52. Gupta, R.K.; Vijayan, D.; Prasad, T.S. New hyperspectral vegetation characterisation parameters. *Adv. Space Res.* **2001**, *28*, 201–206. [CrossRef]
53. Haboudane, D.; Miller, J.R.; Pattey, E.; Zarco-Tejada, P.J.; Strachan, I.B. Hyperspectral vegetation indices and novel algorithms for predicting green LAI of crop canopies: Modeling and validation in the context of precision agriculture. *Remote Sens. Environ.* **2004**, *90*, 337–352. [CrossRef]
54. Broge, N.H.; Leblanc, E. Comparing prediction power and stability of broadband and hyperspetral vegetation indices for estimation of green leaf area index and canopy chlorophyll density. *Remote Sens. Environ.* **2000**, *76*, 156–172. [CrossRef]
55. Gitelson, A.A.; Merzlyak, M.N.; Chivkunova, O.B. Optical properties and nondestructive of anthocyanin content in plant leaves. *Photochem. Photobiol.* **2001**, *74*, 38–45. [CrossRef] [PubMed]
56. Rondeaux, G.; Steven, M.; Baret, F. Optimisation of Soil-Adjusted Vegetation Indices. *Remote Sens. Environ.* **1996**, *55*, 95–107. [CrossRef]
57. Clevers, J.G. Imaging spectrometry in Agriculture: Plant Vitality and Yield indicators. In *Imaging Spectrometry: A Tool for Environment Observations*; Hill, J., Megier, J., Eds.; Kluwer Academic: Dordrecht, The Netherlands, 1994; pp. 193–219.
58. Cohen, J.A. Coeficiente of agrément for nominal scales. *Educ. Psychol. Meas.* **1960**, *20*, 37–46. [CrossRef]
59. Hudson, W.D.; Ramm, C.W. Correct formulation of the kappa coeficiente of agrément. *Photogramm. Eng. Remote Sens.* **1987**, *53*, 421–422.
60. Congalton, R.G.; Green, K. *Assessing the Accuracy of Remotely Sensed Data: Principles and Practices*; Lewis Publishers: Boca Raton, FL, USA, 1999; p. 137.
61. Landis, J.R.; Koch, G.G. The measurement of observer agreement for categorical data. *Biometrics* **1997**, *33*, 159–174. [CrossRef]
62. Gates, D.M.; Keegan, H.J.; Scheletes, J.C.; Weidner, V.R. Spectral properties of plants. *Appl. Opt.* **1985**, *4*, 11–20. [CrossRef]
63. Chen, H.; Wang, P.; Li, J.; Zhang, J.; Zhong, L. Canopy spectral reflectance feature and leaf water potential of sugarcane inversion. *Phys. Procedia* **2012**, *25*, 595–600. [CrossRef]
64. Rabideau, G.S.; French, C.S.; Holt, A.S. The absorption and reflection spectra of leaves, chloroplast suspensions, and chloroplast fragments as measured in an Ulbricht sphere. *Am. J. Bot.* **1946**, *33*, 769–777. [CrossRef]
65. Hall, D.O.; Rao, K.K. *Photosynthesis*; Editora Pedagógica e Universitária: São Paulo, Brazil, 1980; p. 89, ISBN 85-12-92100-5. (In Portuguese)
66. Krezhova, D.; Dikova, B.; Maneva, S. Ground based hyperspectral remote sensing for disease detection of tobacco plants. *Bulg. J. Agric. Sci.* **2014**, *20*, 1142–1150.

67. Jones, C.D.; Jones, J.B.; Lee, W.S. Diagnosis of spot of tomato using spectral signatures. *Comput. Electron. Agric.* **2010**, *74*, 329–335. [CrossRef]
68. Chapelle, E.W.; Mcmurtey, Y.E.; Kim, M.S. Laser induced blue fluorescence in vegetation. In Proceedings of the 10th Annual International Symposium on Geoscience and Remote Sensing, College Park, MD, USA, 20–24 May 1990; Volume 3, pp. 1919–1922.
69. Lang, M.; Stober, F.; Lichtenthaler, H.K. Fluorescence emission spectra of plant leaves and plant constituents. Fluorescence emission spectra of plant leaves and plant constituents. Radiation and Environ. *Biophysics* **1991**, *3*, 333–347.
70. Raven, P.H. *Biologia Vegetal*; Editora Guanabara Koogan: Rio de Janeiro, Brazil, 1997; p. 830, ISBN 978-85-277-1229-3. (In Portuguese)
71. Sims, D.A.; Gamon, J.A. Relationships between leaf pigment content and spectral reflectance across a wide range of species, leaf structures and developmental stages. *Remote Sens. Environ.* **2002**, *81*, 337–354. [CrossRef]
72. Jackson, R.D. Remote sensing of biotic and abiotic plant stress. *Annu. Rev. Phytopathol.* **1986**, *24*, 265–287. [CrossRef]
73. Puchades, Y.; O, M.L.; Montalván, J.; Carvajal, O.; Martínez, Y.; Zardón, M.A.; Mesa, J.M.; Lissbrant, S.; Arencibia, A.D. Genetic and symptomatic characterisation of *Sugarcane mosaic vírus* (SCMV) in Cuba. *Sugar Tech* **2016**, *18*, 184–191. [CrossRef]
74. Lodish, H.; Berk, A.; Kaiser, C.A.; Krieger, M.; Scott, M.P.; Bretscher, A.; Ploegh, H.; Matsudaira, P. *Molecular Cell Biology*; W.H. Freeman and Company: New York, NY, USA, 2000.
75. Gamon, J.A.; Penuelas, J.; Field, C.B. A Narrow-Waveband Spectral Index That Tracks Diurnal Changes in Photosynthetic Efficiency. *Remote Sens. Environ.* **1992**, *41*, 35–44. [CrossRef]
76. Gamon, J.A.; Serrano, L.; Surfus, J.S. The Photochemical Reflectance Index: An Optical Indicator of Photosynthetic Radiation Use Efficiency Across Species, Functional Types and Nutrient Levels. *Oecologia* **1997**, *112*, 492–501. [CrossRef] [PubMed]
77. Johnson, R.M.; Viator, R.P.; Veremis, J.C.; Richard, E.P., Jr.; Zimba, P.V. Discrimination of sugarcane varieties with pigments profiles and high resolution, hyperspectral leaf reflectance data. *J. Am. Soc. Sugar Cane Technol.* **2008**, *28*, 63–75.
78. Grisham, A.P.; Johson, R.M.; Zimba, P.V. Detecting Sugarcane yellow leaf virus infection in asymptomatic leaves with hyperspectral remote sensing and associated leaf pigment changes. *J. Virol. Methods* **2010**, *167*, 140–145. [CrossRef] [PubMed]